THE ASTROPHYSICAL JOURNAL, 420:558–569, 1994 January 10

COUNTERROTATING GASEOUS DISKS IN NGC 4826

ROBERT BRAUN,[1,2] RENÉ A. M. WALTERBOS,[2,3] ROBERT C. KENNICUTT, JR.,[2,4] AND LINDA J. TACCONI[5,6]
Received 1993 April 30; accepted 1993 July 20

ABSTRACT

Observations are presented of the system of nested counterrotating gaseous disks discovered in NGC 4826. Imaging spectroscopy in neutral hydrogen has been done using the VLA and the WSRT. Broad-band optical images in *B*, *V*, and *I* as well as narrow-band images in Hα and [S II] have been obtained at the KPNO. Partial imaging along two position angles in the CO (3 → 2) transition was carried out at the JCMT. All components for which kinematic data exist (neutral, molecular and ionized gas as well as a stellar component) within a radius of 1 kpc share the same sense of rotation. The inner gas disk has an extremely high gas surface density (greater than 50 $M_\odot$ pc^{-2}) and high star formation rate. This inner disk is bounded by an annular region of low gas surface density with faint, diffuse Hα emission detected between 1 and 2.8 kpc radius. An outer gas disk is detected in neutral hydrogen extending from 1.5 to 11 kpc radius at a surface density of ∼0.5 $M_\odot$ pc^{-2}. The H I kinematics indicate counterrotation of this component relative to the inner galaxy at an identical kinematic position angle and inclination. A luminous stellar disk dominates the optical continuum emission and extends out to a radius of 5.5 kpc with substantial surface brightness. Recent optical spectroscopy has shown that the outer stellar disk shares the kinematics of the inner galaxy. It seems likely that the stellar disk decelerates the tenuous, co-planar, counterrotating outer gas disk through a strong interaction with its stellar mass loss. The observed system of nested, counterrotating gaseous disks may have arisen in the antiparallel spin merger of a gas poor spiral with a star-poor dwarf, each containing a few times 10^8 $M_\odot$ of gas. An alternate formation scenario calls for the continuous accretion of a few times 10^8 $M_\odot$ of antiparallel spin gas. The interaction of gaseous disks with stellar mass loss may also play an important role in the evolution of polar ring galaxies as well as more generally in bulge-dominated galaxies.

Subject headings: galaxies: individual (NGC 4826) — galaxies: kinematics and dynamics — galaxies: stellar content — radio lines: galaxies

1. INTRODUCTION

There is a growing realization that the internal kinematics of even apparently normal early-type galaxies are often characterized by multiple distinct subsystems. These can take the form of significantly misaligned rotation of a central stellar component with respect to the main stellar component of the galaxy (Franx, Illingworth, & Heckman 1989; Bender 1990), a gaseous component (often at relatively large radius) which is kinematically distinct from the main stellar component (Schweizer, Van Gorkom, & Seitzer 1989; Bertola et al. 1990), or even multiple gaseous and stellar components. A particularly interesting case in this regard is that of NGC 4550, an E7/S0 galaxy containing an inner gaseous component (with associated stellar absorption) which is counterrotating relative to an extended stellar disk (Rubin, Graham, & Kenney 1992; Rix et al. 1992). These circumstances may be related to the class of violently interacting systems which appear to be the result of mergers or satellite captures, like NGC 7252 (Schweizer 1982, 1993). If kinematic substructure in the stellar population of early-type galaxies is indeed the "fossil" of a major merger event it would be reassuring to find examples of partially processed mergers in which kinematic sub-structure were still visible in the gas.

In this paper we expand on the serendipitous discovery of such a galaxy, the first yet identified with two well-defined counterrotating *gaseous* disks. A brief report of this result has been given by Braun, Walterbos, & Kennicutt (1992, hereafter BWK92). This remarkable circumstance is found within the otherwise normal galaxy NGC 4826 which is classified as an early type spiral [Sab(s)II; Sandage & Tammann 1981].

NGC 4826 (Messier 64), is both nearby (D = 3.8 Mpc after correcting for Virgocentric infall and with H_0 = 100 km s^{-1} Mpc^{-1}) and relatively isolated. The galaxy lies at the outskirts of the loose group CVn I (de Vaucouleurs 1975), which includes NGC 4736 (M94) and ∼15 other possible members. Most of the group members are spirals and irregulars which are spread over an area of 1.9 × 0.9 Mpc and a velocity range of 300 km s^{-1}. No nearby companions (within a few degrees) of NGC 4826 have yet been identified. A distinguishing feature of the galaxy is the prominent dust-lane pattern on the north-eastern side (illustrated in Fig. 7 below) which has given rise to various nicknames such as the "Black-Eye" or "Evil-Eye" galaxy. We observed NGC 4826 as part of a sample of eleven nearby galaxies in a program designed to detect and resolve the major concentrations of neutral and ionized gas. Previous work on Messier 31 (Braun 1990; Braun & Walterbos 1992) had revealed that the major concentrations of neutral gas could be resolved with a linear resolution of ∼100 pc and a velocity resolution of ∼5 km s^{-1}. The resolved structures in M31 have brightness temperatures of up to 180 K, far exceeding that of any structure in our own Galaxy. Combined with detections of H I absorption along a number of lines of sight,

[1] Netherlands Foundation for Research in Astronomy, Postbus 2, 7990 AA Dwingeloo, The Netherlands.
[2] Visiting Astronomer, Kitt Peak National Observatory.
[3] Department of Astronomy, New Mexico State University, Box 30001/Department 4500, Las Cruces NM 88003.
[4] Steward Observatory, University of Arizona, Tucson, AZ 85721.
[5] Max-Planck Institut für Extraterrestrische Physik, Giessenbach Strasse, W-8046 Garching, Germany.
[6] Visiting Astronomer, The James Clerk Maxwell Telescope.

these data indicated a systematic increase of H I spin temperature with radius changing from 70 K at a radius of 7 kpc to 180 K at 15 kpc in M31. We hoped to probe the physical conditions of the neutral gas in a sample of the nearest external galaxies over an even wider range of radius, metallicity, interstellar pressure, and dust content. As will become clear in this first paper describing the results of this program we have certainly succeeded in broadening our scope. Observations we have obtained of NGC 4826 and the data reduction are presented below in § 2, followed by a description and discussion of the results in §§ 3 and 4.

2. OBSERVATIONS

2.1. *Neutral Hydrogen Observations*

Neutral hydrogen observations of NGC 4826 were obtained with the VLA[7] between 1989 March and 1990 November. The B, C, and D configurations (with effective integration times of 7, 0.5, and 0.5 hr) were utilized to image a region 0°.5 in diameter at 6″ resolution. In addition, a small hexagonal mosaic in the D configuration (with 0.5 hr effective integration on each of seven positions) was used to image a 1° diameter field at 65″ resolution. Standard calibration and imaging techniques were used to produce a series of narrow-band images separated by 5.15 km s^{-1} over a velocity range of 660 km s^{-1} centered on 415 km s^{-1}, the nominal heliocentric systemic velocity of NGC 4826. A continuum image, formed from the average of line-free channels (150–250 and 580–680 km s^{-1}) was subtracted from each image. A simultaneous deconvolution based on the Maximum Entropy Method (as in Cornwell 1988) was carried out on the seven pointings of the low-resolution mosaic to determine the smoothest model brightness distribution at each velocity consistent with the data (corrected for primary beam attenuation) and the measurement noise. The model brightness distributions were then convolved with a two-dimensional Gaussian fit to the instrumental response; to which were added the residuals of the deconvolution. Since the zero level of each narrow-band image remains unconstrained due to the absence of total power data, the mean brightness in a region outside of the source was then subtracted from each. The good response to extended structure (as large as ~30′) obtained in this low-resolution mosaic was incorporated into the series of high-resolution images by replacing the inner Fourier plane of each (as in Braun 1988). Smoothing of the high-resolution (6″) data cube to resolutions of 9″ and 15″ was necessary before significant line emission could be detected. A continuum image was made from the outlying line channels with ~1 MHz of total bandwidth.

Additional observations in the neutral hydrogen line were obtained with the Westerbork Synthesis Radio Telescope (WSRT) during 1992 September. Twelve hours of integration were obtained on each of September 2, 6, 10, and 11 providing complete, repeated sampling and tracking of east-west baselines from 36 to 2880 m with an increment of 36 m. Standard calibration and imaging techniques were used to produce a series of narrow-band images separated by 4.13 km s^{-1} over a velocity range of 460 km s^{-1} centered on 415 km s^{-1}. Continuum emission was identified and subtracted directly from the visibility data before imaging by fitting linear functions to the Cosine and Sine channels over the line-free velocity intervals (167–246 and 569–626 km s^{-1}). Gaussian tapering of the visibilities after weighting proportional to baseline length was used to obtain data-cubes with 35″, 60″, and 120″ spatial resolution. Each narrow-band image was deconvolved with the CLEAN algorithm down to a limiting flux of ~4 mJy beam^{-1} corresponding to twice the rms fluctuation level.

[7] The VLA is a facility of the National Radio Astronomy Observatory, which is operated by Associated Universities, Inc., under contract with the National Science Foundation.

2.2. *Narrow- and Broad-Band Optical Observations*

Optical observations of NGC 4826 were obtained in 1989 February with the No. 1 36 inch (0.9 m) and in 1989 May with the Burrell Schmidt telescope at the Kitt Peak National Observatory. Exposures of a 6°.6 square field were obtained in a 38 Å band centered on the Hα emission line and a 75 Å continuum band centered at 6649 Å using a CCD camera equipped with the Tek 1 chip on the No. 1 36 inch telescope. A similar camera set-up on the Burrell Schmidt telescope was used to image a 22′ square field in the standard *B*, *V*, and *I* bands as well as in 75 Å bands centered on the Hα + [N II] emission lines, the [S II] λλ6717, 6731 emission lines and a continuum band centered at 6649 Å. Standard flat-fielding and calibration methods were used in reducing the data. Astrometry of the exposures was carried out using the HST-GSC positions (precessed to B1950) of seven stars in the 6°.6 square fields and 11 stars in the 22′ square fields. Solution residuals were less than ~0″.2 and 0″.5 in the small and large fields, respectively. From our imagery we derive the position of peak optical continuum emission to be $\alpha_{1950} = 12^h54^m16^s.34$, $\delta_{1950} = 21°57'11''.8$ with ~0″.5 precision.

2.3. CO *Observations*

We made observations of the $J = 3 \rightarrow 2$ transition of ^{12}CO in 1992 June using the 15 m James Clerk Maxwell Telescope (JCMT) on Mauna Kea, Hawaii. At the 345 GHz frequency of the CO line, the beam diameter of the JCMT is 15″. We mapped the CO emission at seven positions along an east-west line and two additional positions to the north and south of a reference position which was displaced by ~7″.5 east and 6″ north of the nucleus of NGC 4826. To obtain the spectra we used a 345 GHz SIS receiver with a noise temperature of 150 K (DSB) as the frontend. The system temperature referred to the top of the atmosphere was ~900 K (SSB). The back end was an acousto-optical spectrometer with a bandwidth of 500 MHz and an effective frequency resolution of 0.45 MHz. The data were taken in a beam-switching mode using the chopping secondary, a chop frequency of 1 Hz, and a chop throw of 2′ in azimuth.

The antenna temperature scale was calibrated using an ambient temperature chopper-wheel to remove first order atmospheric and telescope losses. We measured the main beam efficiency (η_{mb}), the fraction of the forward power in the main beam, by observing planets and found it to be 0.42. Telescope pointing and focus were checked frequently by observing planets. The overall pointing accuracy was good to ~3″ rms. Total integration times of between 1200 and 4300 s were obtained at the various positions, except the position (8, −4″) where only 300 s of integration were obtained.

3. RESULTS

3.1. *Large-Scale Structure of Neutral Hydrogen*

Velocity-fields were determined for the neutral hydrogen emission in each of the data cubes (at the various resolutions)

by forming an image of the velocity corresponding to the brightest measured emission along each line of sight. This is in contrast to, and in many ways superior to, the commonly employed technique of forming moment images from a filtered version of the data. The resulting velocity-fields were "blanked" (declared undefined) outside the connected regions where significant emission was detected. The velocity-field derived from the 65″ VLA mosaic is shown in Figure 1. A color representation of this figure was presented in BWK92. A disk of 22′ diameter is detected at this resolution. This is similar in extent to that detected previously (Van Driel & Buta 1991) at a comparable resolution. The more extended spatial coverage of the hexagonal mosaic has revealed at least one additional component of emission situated $\sim 10'$ south of this extended disk (at velocity 550 km s^{-1}). Smoothing the (single pointing) WSRT database to 120″ resolution reveals the continuous low brightness extension ($N_H \sim 10^{19}$ cm^{-2}) indicated by the broken line in Figure 1 which joins the extended disk to this fragment. The decreasing sensitivity at large radii of these data do not allow us to determine the complete extent of this tail. Contours of integrated H I emission at 120″ resolution are overlaid on our broad-band B frame in Figure 2. A relatively smooth gaseous disk extends out to about twice D_{25} (D_{25} = 10.′2). Fitting a tilted ring model with free parameters of rotation velocity, inclination and position angle of the receding line-of-nodes (as in Begeman 1989) to the observed (65″ resolution) velocity-field between 100″ and 750″ (1.8 and 14 kpc) radius yields the kinematic parameters shown in Figure 3 (after solving for the mean kinematic center and systemic velocity). A severe distortion is observed between 100″ and 300″ radius, followed by a well-modeled disk rotating at velocity 150 km s^{-1} at an inclination near 60° with a receding line-of-nodes at P.A. 125°. (We will address the distortion noted here briefly below and in greater detail in § 4.4.) The total line flux we detect is 39.6 ± 0.4 Jy km s^{-1} corresponding to an (optically thin) mass, $M_{HI} = 1.33 \times 10^8\ M_\odot$. Total

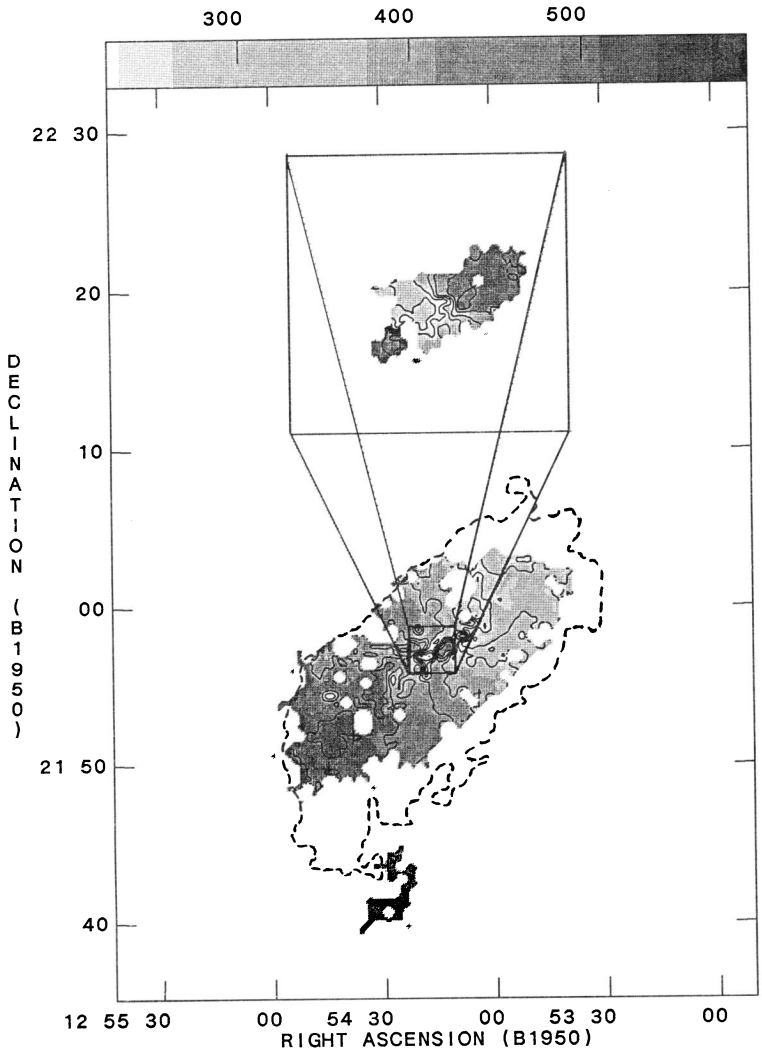

FIG. 1.—Line-of-sight velocity of neutral hydrogen emission in NGC 4826. The gray-scale extends from 225 to 595 km s^{-1} and isovelocity contours are drawn at 250–550 km s^{-1} in steps of 50 km s^{-1}. Note the "spider pattern" characteristic of differential rotation, with the highest receding velocities observed along a position angle of 125° (east of north) in the outer disk (shown at 65″ resolution). The sense of rotation is observed to reverse within the central region of the galaxy, as seen in the 15″ resolution inset to the figure. At intermediate radii (between 100″–300″) there is an S-shaped distortion in the outer disk. Note also the feature 10′ south of the outer disk with velocity similar to the disk velocity at that position angle. The dashed contour represents the maximum extent of emission detected at a resolution of 120″.

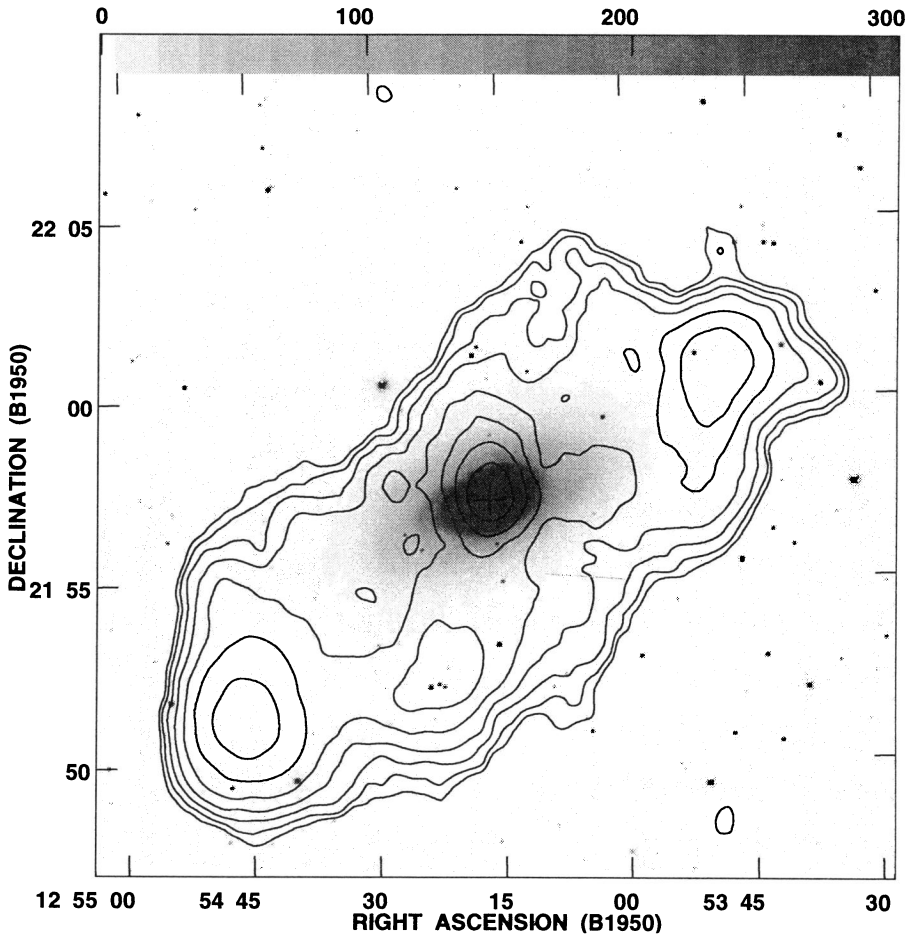

FIG. 2.—Integrated H I emission of NGC 4826 overlaid on the blue optical continuum. Contours of H I column density (assuming low optical depth) at a resolution of 120″ are drawn at 2, 2.8, 4, 5.6, 8, 11.2, 16, and 22.4 × 10^{19} cm^{-2}. Note the relatively smooth disk extending out to about twice D_{25} (D_{25} = 10.2), and the central maximum due to the inner gas disk with an opposite sense of rotation.

power measurements of the line flux (e.g., Tully & Fisher 1981) agree with our determination to within 5%.

3.2. *Small-Scale Structure*

3.2.1. *Neutral and Molecular Gas Properties*

An unusual aspect of the integrated H I distribution shown in Figure 2 is the peak of emission seen toward the nucleus. This is more clearly illustrated in Figure 4 where the average H I column density is shown as a function of semimajor distance for elliptical annuli centered on the nuclear position, elongated at P.A. 120° and having a major to minor axis ratio of 2. Column densities of a few times 10^{21} cm^{-2} are seen in the inner 20″, followed by a local minimum between 60″ and 90″, subsequent disk emission near a column of 10^{20} cm^{-2} between 100″ and 500″ and a final decline to below 10^{19} cm^{-2} by ~700″. Central *depressions* in the neutral gas surface density are much more frequently observed in normal galaxies. A closer inspection of the central region of the galaxy reveals that it is peculiar in a number of other respects. In particular, the sense of rotation is observed to *reverse* in the central region of 2′ (corresponding to 2 kpc) diameter. Although this is already apparent in the 65″ resolution data, this central region is best seen at the higher angular resolution (15″) of the inset to Figure 1. Fitting a tilted ring model to the (15″ resolution) velocity field between 12″ and 60″ yields the kinematic parameters illustrated in Figure 3 (after solving for the mean kinematic center and systemic velocity). The rotation velocity is observed to decrease from ~180–150 km s^{-1} at an inclination which varies smoothly from ~50° to 70° with a receding line-of-nodes at P.A. −65°, i.e., opposite to that of the outer galaxy. The two nested systems are easily seen in the position-velocity diagram of Figure 5 which was taken through the nucleus along P.A. −55° in the WSRT data at 60″ resolution. Position-velocity diagrams above and below the major axis do not show obvious evidence of interaction between these two systems but instead show the larger-scale symmetric distortion noted above which is distinctly seen at plus and minus 2′ minor axis offset (also in Fig. 5). Apart from localized irregularities, there are no indications for the presence of multiple velocity components occurring at similar radii in the galaxy. (This would of course be extremely unlikely for a gaseous disk.)

Our CO spectra from the inner region of the galaxy are shown in Figure 6, plotted on the main beam brightness temperature scale. Although the spatial coverage is far from complete, it is clear that the highest recession velocities of ~560 km s^{-1} are observed in the west and the lowest of ~280 km s^{-1} in the east. The magnitude and sense of rotation of the molecular gas is therefore fully consistent with that of the inner neutral hydrogen disk. The CO brightness distribution, although concentrated to the inner galaxy, appears to peak at a radius of ~10″–15″ rather than toward the nucleus itself, and then

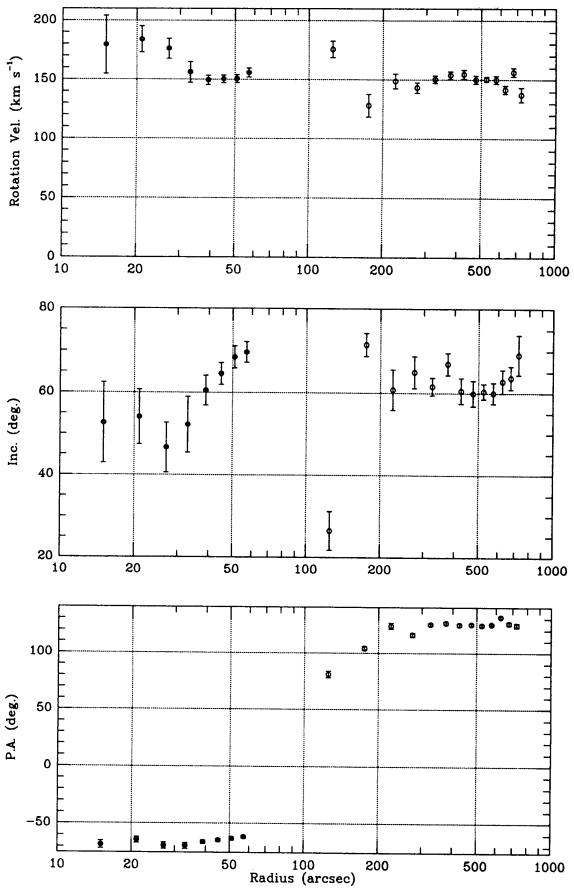

FIG. 3.—Kinematic parameters of the counterrotating neutral hydrogen disks. Rotation velocity (*top*), inclination (*middle*), and position angle (*bottom*) as a function of radius for the inner disk (*filled symbols*) and the outer disk (*open symbols*) systems, as determined from fitting a tilted ring model to the radial velocities shown in Fig. 1. Note the similar kinematic inclination and rotation velocity but diametrically opposed position angle of the receding line of nodes. Also note the severe distortion between 100″ and 200″ radius where the solution parameters vary in an unphysical way.

becomes significantly fainter at a radius of ~30″. The brightness profile of the molecular gas (at least in the $J = 3 \rightarrow 2$ transition of ^{12}CO) is therefore also consistent with that of the neutral hydrogen, as illustrated in Figure 4.

3.2.2. *Ionized Gas Properties*

An overview of a number of the emission components in the inner galaxy is given in Figure 7 (Plate 10). The prominent absorption band system visible in the optical continuum is co-extensive with a disk undergoing massive star formation as seen in both Hα and the radio continuum. The magnitude and sense of rotation of this system has been determined through high-velocity resolution optical spectroscopy of the H II regions in the Hα and [N II] emission lines (Rubin et al. 1965) and is consistent with the high spatial resolution H I and CO velocity fields. Although only limited stellar spectroscopy has been published a stellar component with the same sense of rotation has been observed between 3″ and 30″ radius (Walker 1989). A preliminary presentation of more recent stellar spectroscopy at radii less than 7″ (Kormendy 1992) was not accompanied by any comment of peculiarities. Our own deep stellar spectroscopy, carried out in 1993 April (Rix et al. 1994), traces the stellar kinematics out to a radius of 120″ and reveals only a single stellar component with consistent kinematic properties. All of the components for which kinematic data exist in the inner galaxy share the same sense of rotation which is opposite to that of the gas in the outer galaxy. The detailed correspondence of neutral and ionized gas in the inner galaxy is illustrated in Figure 8. The integrated H I emission at 15″ resolution is very well correlated with the Hα emission; sharing a ringlike concentration at 15″ radius, a disk extending out to 60″ and a marked asymmetry from northwest to southeast. This similarity argues against a large component of differential extinction accounting for the asymmetric morphology of the Hα disk. (Indeed, spectroscopy of the H II regions obtained by R. C. K. suggests a mean extinction of 1.5 mag and metal abundances of 1–2 times solar with no systematic variation with position.) The H I velocity field is generally consistent with differential rotation, as noted above, but two regions of large, organized departures (of ~100 km s^{-1}) from circular rotation are apparent immediately to the north of the nucleus and ~15″ to the southwest. These departures are aligned with arcs in the Hα distribution and as such are reminiscent of spiral arms at larger radii in other galaxies. Systematic departures of a similar magnitude (up to 70 km s^{-1}) are seen in the central kpc of Messier 31 (e.g., Braun 1991).

Also visible in the Hα images of Figures 7 and 8 is an elongated circumnuclear structure of 8″ extent. (The apparent deficit of emission towards the nucleus itself is due to localized blanking in one of the No. 1 36 inch exposures.) From both the No. 1 36 inch and Burrell Schmidt sets of images we estimate the contribution of this structure to the integrated Hα line flux to be 8%. Comparison with our imagery in [S II] indicates that this circumnuclear structure has a [S II] to Hα line ratio of ~1.5, consistent with its LINER classification by Keel (1983). In Figure 9 we show a high contrast image of the Hα emission from the central region of the Burrell Schmidt frame. The relatively bright inner disk which extends out to a radius of 55″ is surrounded by a region of low surface brightness arcs out to a (deprojected) radius of 150″, particularly in the northeast and

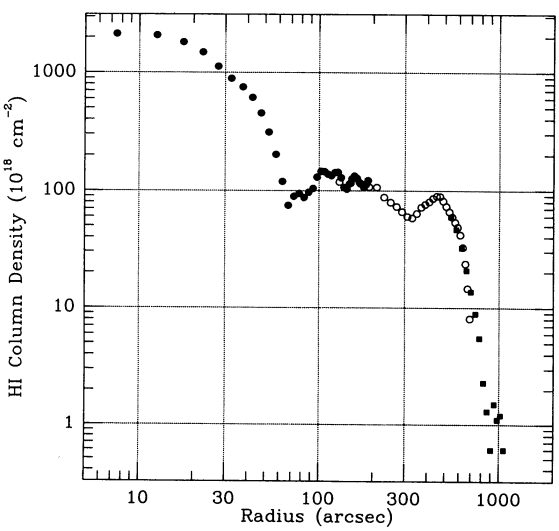

FIG. 4.—Column density profile of neutral hydrogen emission. The column density of H I (assuming low optical depth) obtained from averaging in elliptical annuli elongated at P.A. 125° and with a major to minor axis ratio of two using 15″ resolution data (*filled circles*), 60″ resolution data (*open circles*), and 120″ resolution data (*filled squares*). Face-on surface densities of H I in $M_\odot$ pc^{-2} can be obtained by scaling with a factor 4.0×10^{-21} cm^2.

PLATE 10

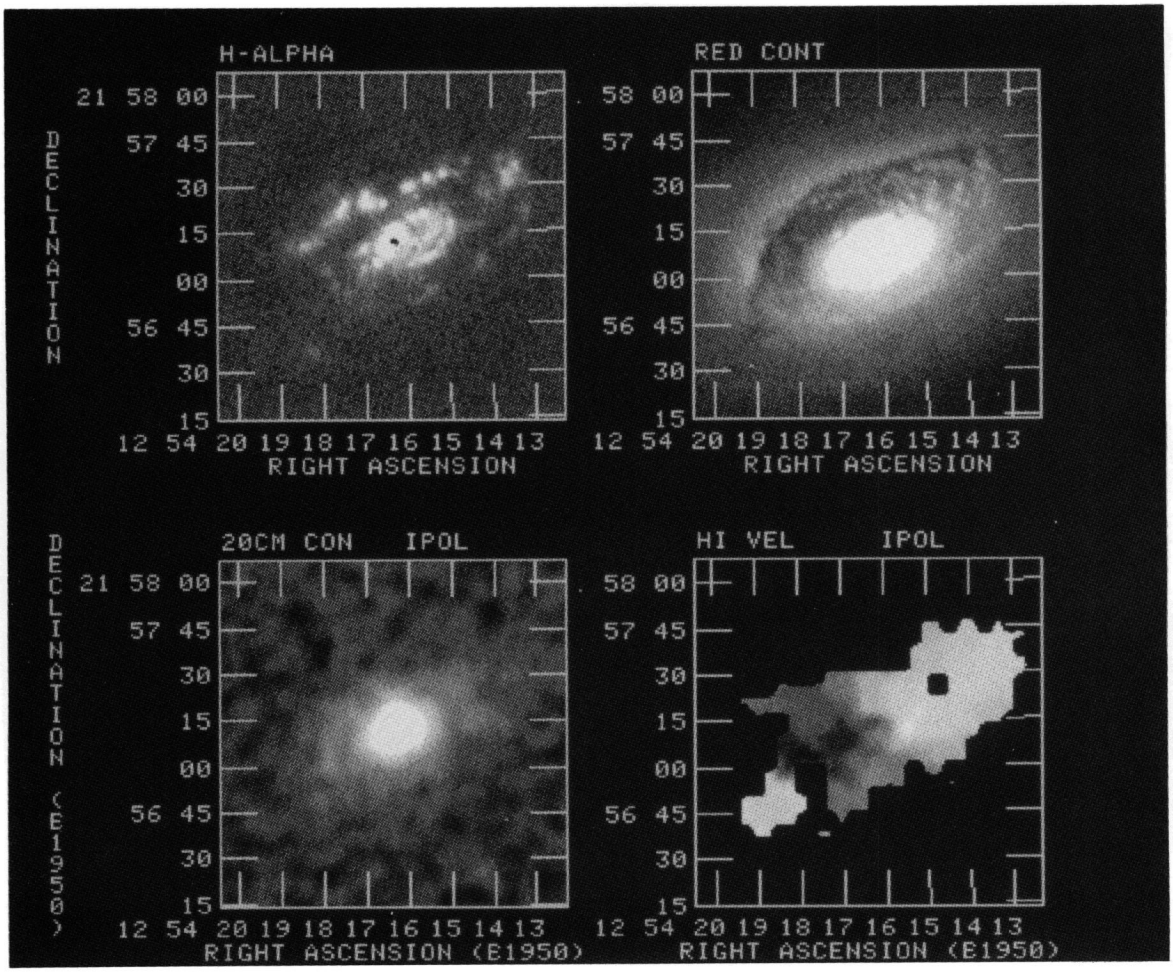

FIG. 7.—Emission, absorption, and kinematics of the inner region of NGC 4826. From left to right and top to bottom: narrow-band optical imagery in Hα + [N II], optical continuum in a 75 Å band centered at 6649 Å, radio continuum emission at $\lambda = 20$ cm, and the line-of-sight velocity of neutral hydrogen emission. The prominent dust lanes are coextensive with the bright Hα, CO, and H I which all rotate in the opposite sense to the diffuse H I disk at larger radii.

BRAUN et al. (see 420, 562)

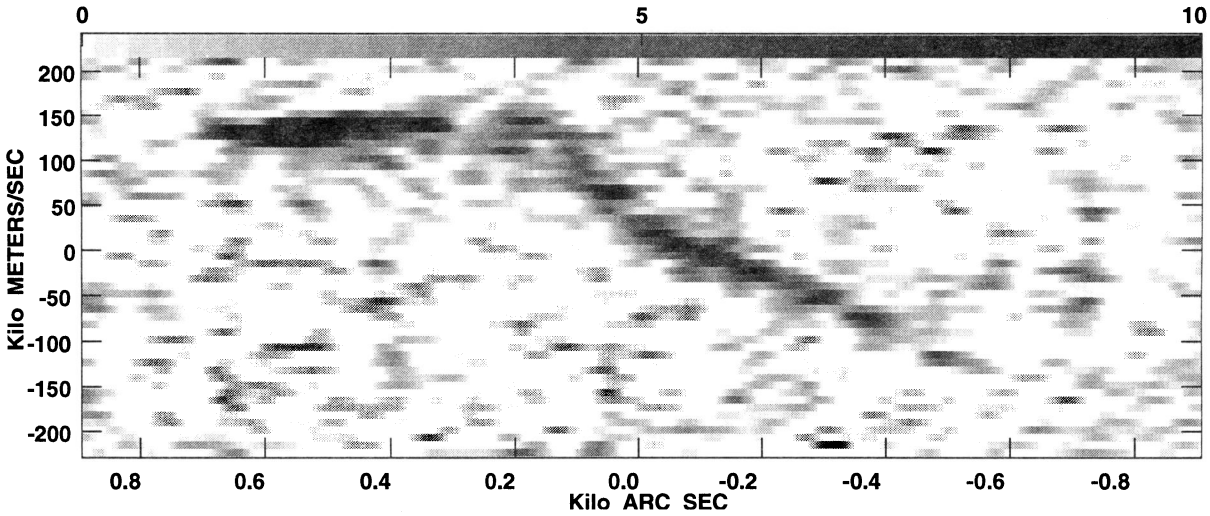

FIG. 5a

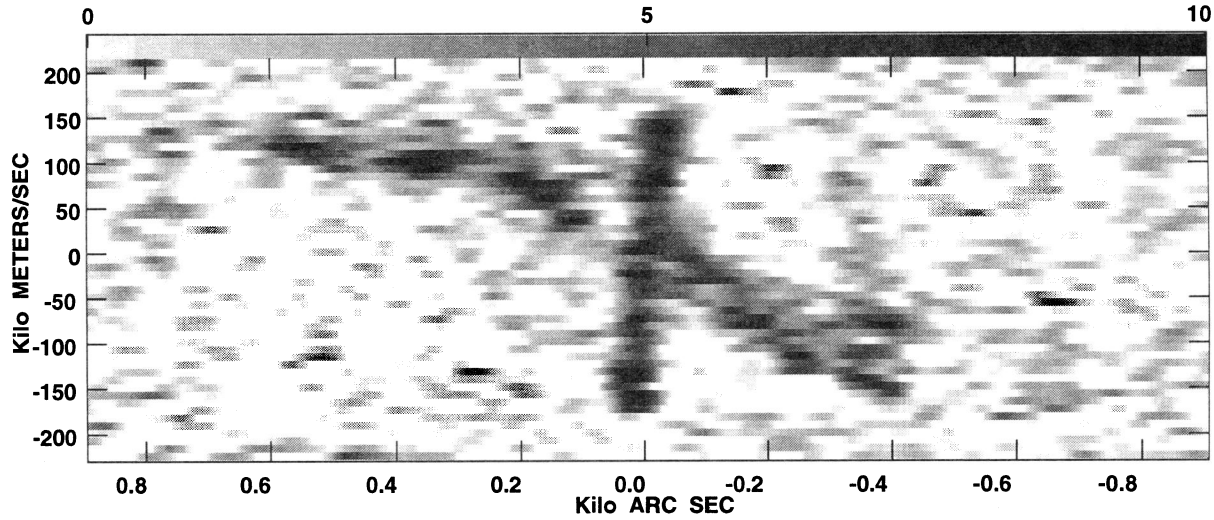

FIG. 5b

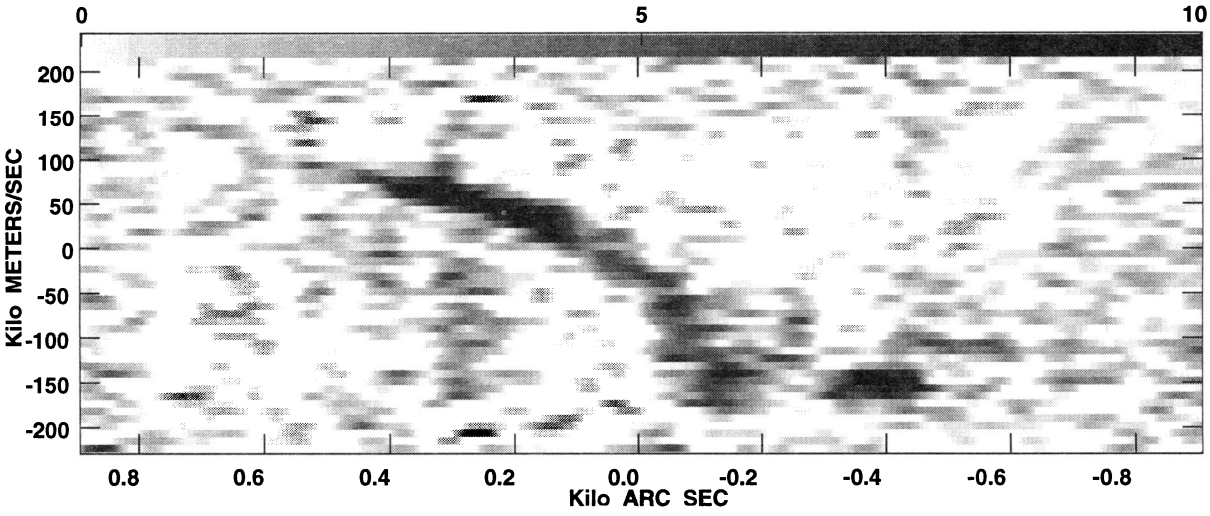

FIG. 5c

FIG. 5.—Position-velocity diagrams of H I emission parallel to the major axis (along P.A. 125°) at a resolution of 60″ and offset by (*a*) 2′ to the northeast, (*b*) 0′, and (*c*) 2′ to the southwest. Positive position offsets increase to the southeast and the velocity is relative to a systemic velocity of 415 km s^{-1}. The gray scale extends from 0 to 10 mJy $beam^{-1}$, and the data are not corrected for primary beam attenuation. Note the clear signature of the nested, counterrotating system of disks along the major axis in (*b*) and the symmetric departures from the linear pattern expected for pure rotation on either side of the major axis which give rise to the S-shaped distortion seen in Fig. 1.

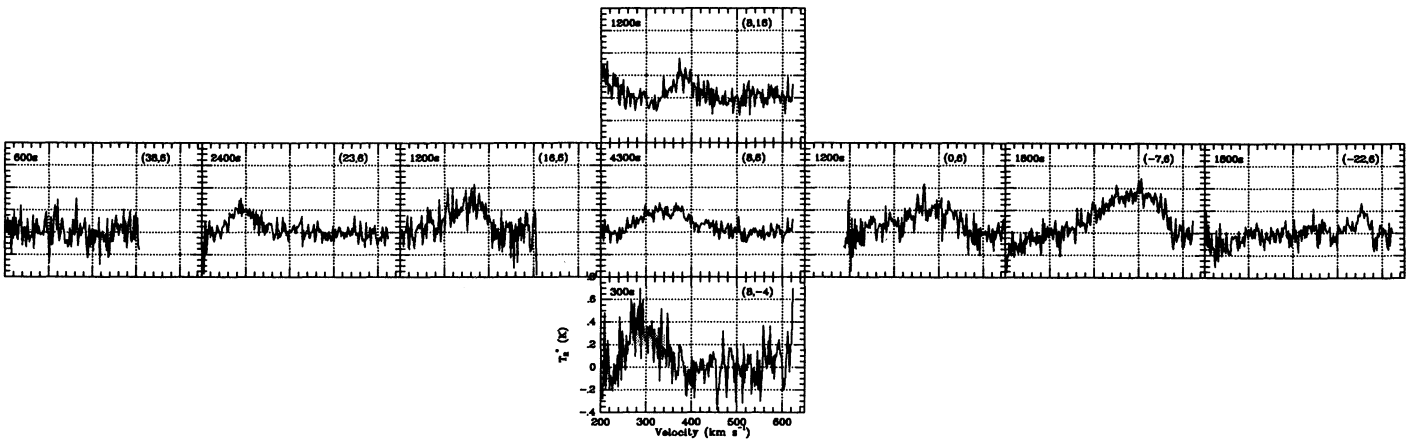

FIG. 6.—Emission spectra of ^{12}CO (3 → 2) from the inner disk of NGC 4826 at a resolution of 15″ on the main beam brightness temperature scale. Offsets in arcseconds from the nuclear position are indicated at upper right. Integration times in seconds are indicated at upper left. Note the agreement in the sense and magnitude of the kinematics with the inner H I disk and the similar distribution.

to the west. The brightest portions of these arcs reach surface brightnesses of only 10^{-16} ergs cm^{-2} s^{-1} arcsec^{-2}. Inside of a 55″ radius the elliptically averaged [S II] to Hα line ratio is in the range 0.2–0.3, consistent with photoionization in normal H II regions (e.g., Walterbos & Braun 1992). Although signal-to-noise is not high, the line ratios are systematically higher between radii of 55″–120″ with average values of 0.7–0.9 occurring between 80″ and 105″. Such ratios of [S II] to Hα are significantly higher than those found in "normal" regions of diffuse ionized gas, for which values of 0.56 ± 0.11 have been found (Walterbos & Braun 1992), and very likely indicate collisional ionization in shocks. At even larger radii there are indications for an extremely low surface brightness Hα halo. Since this apparent halo is at the level of possible residual artifacts in our flat-fielding and continuum subtraction we regard it as extremely uncertain.

3.2.3. *Radio Continuum Properties*

The radio continuum emission, while also well correlated with the ionized gas, is distributed more symmetrically. No compact nuclear component is detected in the radio continuum, but rather a resolved peak with a centroid which is offset to the northwest of the stellar nucleus, much like the distribution of Hα emission. Comparison with images of the nuclear region at a frequency of 1.46 GHz, but with 1.″3 resolution (Hummel et al. 1987), suggests that while the northwest region is partially resolved into compact substructure there is in fact no compact counterpart to the stellar nucleus in excess of ∼0.6 mJy. Elliptically averaged profiles of surface brightness in the 20 cm continuum and in Hα emission track each other quite accurately between radii of ∼5″ and 90″ with the ratio varying between ∼20 and 35 μJy continuum per 10^{-15} ergs cm^{-2} s^{-1} of line emission. At a wavelength of 20 cm the expected optically thin thermal continuum emission for a given line flux in Hα is 1.0 in these units. Assuming an optical extinction at Hα of 1.5 mag, leads one to expect about 4.0 in the ratio for the thermal contribution, corresponding to a thermal fraction between ∼10% and 25%. Although the integrated radio spectrum of NGC 4826 is quite poorly defined at present (see Duric, Bourneuf, & Gregory 1988) there is a substantial nonthermal contribution which yields a spectral index of ∼0.52 between 1 and 5 GHz (from Condon, Frayer, & Broderick 1991) so that the above estimates of the local thermal fraction at 1.4 GHz appear quite plausible. An upper limit to the total thermal fraction at 1.4 GHz of ∼25% would imply a mean extinction at Hα of ∼2 mag.

3.2.4. *Neutral Hydrogen Absorption*

The integrated H I line flux we detect from the inner disk is 3.2 ± 0.1 Jy km s^{-1} corresponding to an (optically thin) mass, $M_{HI} = 1.1 \times 10^7\ M_\odot$. Although the radio continuum emission from the nuclear region seen in Figure 8 is extended, it is sufficiently bright that absorption due to foreground H I could be detected. A circular region of 21″ diameter (corresponding to 390 pc) centered on the continuum source was isolated from each channel of the full resolution (6″) H I database. An elliptical Gaussian of fixed size (18.″2 × 14.″1 FWHM at P.A. 110°) and position (determined from line-free channels) and a zero level were fitted by least-squares to each masked channel image. The normalized (by the peak continuum brightness) height of the elliptical Gaussian measures the line-of-sight absorption, $(e^{-\tau} - 1)$, while the zero level measures the interpolated line-of-sight emission. (For a more extensive discussion of this procedure see Braun & Walterbos 1992). Significant absorption was detected only over the velocity interval 435–470 km s^{-1} shown in Figure 10. Comparison with the velocity field shown in Figure 8 illustrates that gas in this velocity interval crosses the centroid of the continuum emission. (Recall that the centroid of the continuum emission is offset to the northwest of the nucleus.) Since the continuum emission is intrinsic to NGC 4826 and is probably distributed more or less co-spatially with the neutral hydrogen, only a fraction of the H I gas can contribute to the measured absorption, while all of the gas can (in principal) contribute to the measured emission. The indicative spin temperature of 50–60 K (also shown in Fig. 10) obtained from the ratio of total emission brightness to measured absorption is therefore probably an overestimate of the actual spin temperature by as much as a factor of 2. The highest brightnesses observed directly in H I emission at a resolution of 9″ (corresponding to 165 pc) are 35–40 K. These brightnesses may already be due to gas with a significant optical depth in H I. The total H I mass from the inner disk could therefore be larger by a factor of 1.2–2 relative to the optically thin estimate above. The low spin temperatures of H I found in the central kpc of NGC 4826 fit in well with the radial gradient of H I spin temperature found in Messier 31 (Braun &

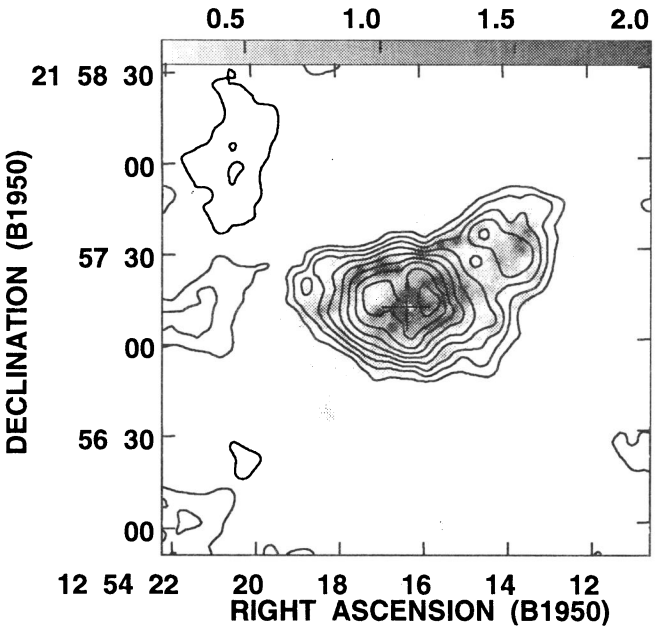

FIG. 8*a*

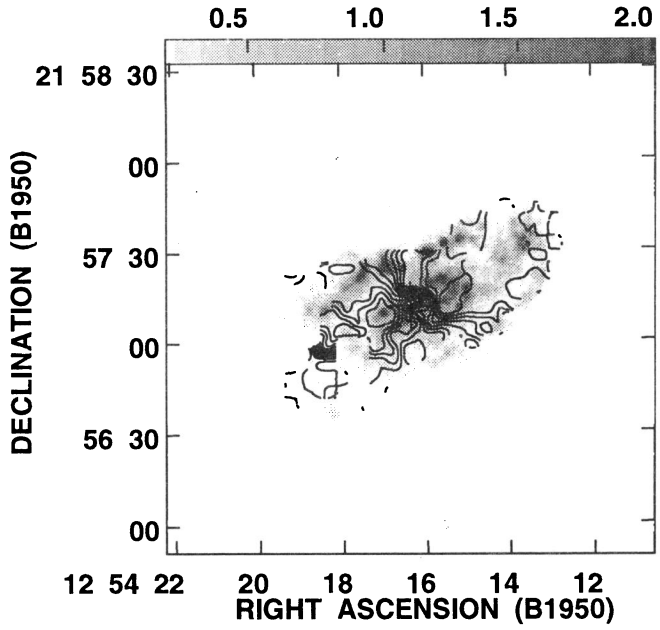

FIG. 8*b*

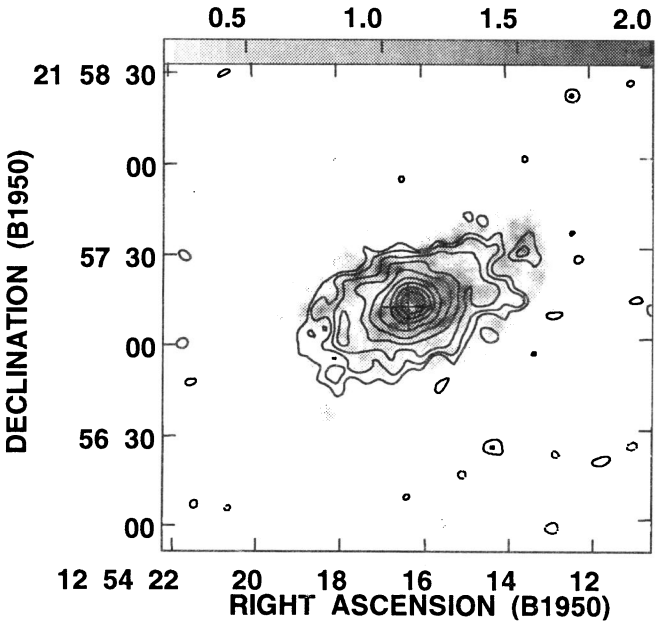

FIG. 8*c*

FIG. 8.—Overlay of neutral hydrogen and radio continuum emission on Hα from the inner disk. On a gray-scale representation of the Hα brightness extending from 0.3 to 3.0 × 10^{-15} ergs cm^{-2} s^{-1} $arcsec^{-2}$ are (*a*) contours of H I column density (assuming low optical depth) at 15″ resolution at 2.5 to 22.5 × 10^{20} cm^{-2} in steps of 5 × 10^{20} cm^{-2}, (*b*) isovelocity counters of H I emission at 15″ resolution at 250–550 km s^{-1} in steps of 25 km s^{-1}, and (*c*) contours of radio continuum brightness at 20 cm wavelength at (−1, 1, 1.4, 2, 2.8, 4. 5.6, 8, 11.2, and 16) × 0.5 mJy per 6″ beam. Note the compact ring (15″ radius) in H I, the good correspondence of H I and Hα including the strong northwest-southeast asymmetry, the localized departures from circular rotation coincident with arcs in Hα and the offset of the radio continuum centroid with respect to the nucleus.

Walterbos 1992). Presumably the enhanced cooling of a high gas-phase metal abundance and high gas pressure win out over the enhanced heating due to a high dust-to-gas ratio and high ionization rate.

4. DISCUSSION

4.1. *Geometry*

As discussed in BWK92, the three-dimensional geometry of the nested disk system cannot be unambiguously determined from the gas kinematics alone. The similar kinematic inclinations of the two disks (illustrated in Fig. 3) implies that the inner and outer system are either aligned to within ∼5° or misaligned by ∼50°. Morphological clues from the enhanced absorption to the northeast at small radii and the faint spiral arms at large radii seem to favor misalignment if the stellar disk shares the kinematics of the outer gas disk. Our recent stellar spectroscopy (Rix et al. 1994) has revealed that the stellar disk has the kinematics of the *inner* gas disk so that this argument for misalignment is no longer relevant. Kinematically, it is much easier to envision stability in the co-planar case. We are presenting a separate analysis of our multicolor broad-band photometry (Walterbos, Braun, & Kennicutt 1994) which seems to favor the case for the inner gas disk being nearly co-planar with the stellar disk. The absolute orientation of the outer gas disk is still an open question, although the discussion below in § 4.4 is most consistent with it also being approximately coplanar with the other components.

4.2. *Gas Content*

As noted above, the outer gaseous disk of NGC 4826 has an H I mass, $M(\mathrm{H\ I}) = 1.33 \times 10^8\ M_\odot$, while the inner disk has $M(\mathrm{H\ I}) = 1.1 \times 10^7\ M_\odot$ under the assumption of low optical depth. In view of the evidence for low gas temperature and substantial opacity in the inner disk, the neutral mass concentrated there may actually be a few times larger. Although complete imaging in CO has not yet been undertaken, our sampling of the inner disk at 15″ resolution suggests that pre-

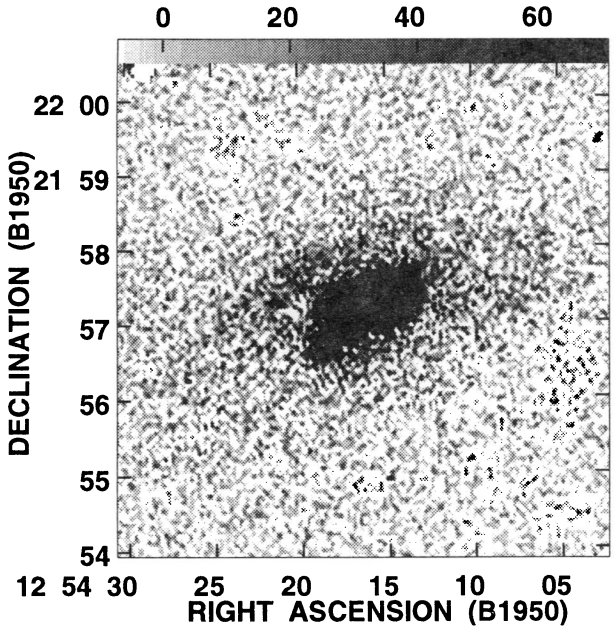

FIG. 9.—High-contrast Hα image of NGC 4826. The central 6.5 of the 22′ field of view of the Burrell Schmidt exposure in Hα. The gray-scale extends from about -10 to 100×10^{-18} ergs cm^{-2} s^{-1} arcsec^{-2}. Note the relatively high surface brightness disk extending to a radius of 60″ and the diffuse low brightness arcs extending to 150″ radius, most prominently in the northeast and west.

vious spectra obtained by Sage & Isbell (1991) with a 55″ beam centered on the nucleus should have been sensitive to most of the dense ($n_H \sim 10^3$–10^4) gas distribution. They report integrated line strengths of 26.4 ± 0.8 K km s^{-1} in ^{12}CO ($1 \rightarrow 0$) and 5.02 ± 0.24 K km s^{-1} in ^{13}CO ($1 \rightarrow 0$). The nominal conversion factor of ^{12}CO ($1 \rightarrow 0$) line strength to molecular column density, 2.3×10^{20} cm^{-2} (K km s^{-1})$^{-1}$ (Bloemen 1989) yields a molecular mass estimate, $M(H_2) = 1.3 \times 10^8$ $M_\odot$. Therefore the total gas mass M(H I + H_2 + He) in the galaxy of $\sim 4 \times 10^8$ $M_\odot$ appears to be split into two components of similar mass, ~47% in the outer disk of 11 kpc (600″) radius and 53% in the inner disk of 1.1 kpc (60″) radius.

Total gas surface densities (including 40% He by mass) are ~ 0.50 $M_\odot$ pc^{-2} in the outer disk and ~ 55 $M_\odot$ pc^{-2} on average in the inner disk.

4.3. *Star Formation Rate*

The extremely high gas surface densities in the inner disk are accompanied by a high rate of massive star formation. High brightness emission in Hα is confined entirely to the inner disk (as seen in Figs. 7, 8, and 9). The integrated line flux we detect over the entire inner disk within the 38 Å filter width of the No. 1 36 inch exposure is 3.9×10^{-12} ergs cm^2 s^{-1}. The filter is well centered on the Hα line (at the redshift of NGC 4826) and includes approximately half the flux of the neighboring [N II] lines. The integrated flux of the Hα + [N II] lines obtained with large aperture photometry (Kennicutt & Kent 1983) is f(Hα + [N II]) $= 4.8 \times 10^{-12}$ ergs cm^2 s^{-1}. Assuming a 30% total contribution of [N II] the two values above give a consistent value of $\sim f(H\alpha) = 3.4 \times 10^{-12}$ ergs cm^2 s^{-1}. Correcting for an 8% nuclear contribution and an average extinction of 1.5 mag (estimated from recent spectrophotometry we have obtained) yields a luminosity $L(H\alpha) = 2.1 \times 10^{40}$ ergs s^{-1}. This luminosity corresponds to an indicative star formation rate (Kennicutt 1983) for the inner disk of 0.19 $M_\odot$ yr^{-1}. The associated gas depletion time scale, assuming 25% recycling of the gas, is 1.4 Gyr. Although the total gas content of the inner disk is rather low, the current rate of massive star formation is quite vigorous. Similar indications follow from a consideration of the infrared luminosity. Soifer et al. (1987) give an integrated infrared luminosity, $L_{IR} = 1.4 \times 10^9$ $L_\odot$ (scaled to the distance assumed here of 3.8 Mpc). This leads to the ratio $L_{IR}/M(H_2) = 11$ $L_\odot/M_\odot$, the same as the median value found by Young & Devereux (1991) for a sample of starburst galaxies and well above the median found in normal isolated galaxies, for which $L_{IR}/M(H_2) = 5$ $L_\odot/M_\odot$. The dust temperature is also indicative of massive star formation since the 60–100 μm flux ratio of 0.45 is higher than that of any of the Sb galaxies in the nearby galaxy sample of Rice et al. (1988).

4.4. *Outer Disk Kinematics*

As noted previously in §§ 3.1 and 3.2, the velocity field of the outer gaseous disk shows a severe distortion at radii between 100″ and 300″. This distortion is reflected in the S-shaped ridge line of maximum positive and negative line-of-sight velocities relative to the systemic velocity (as seen in Fig. 1) as well as the step-function appearance of position-velocity diagrams offset

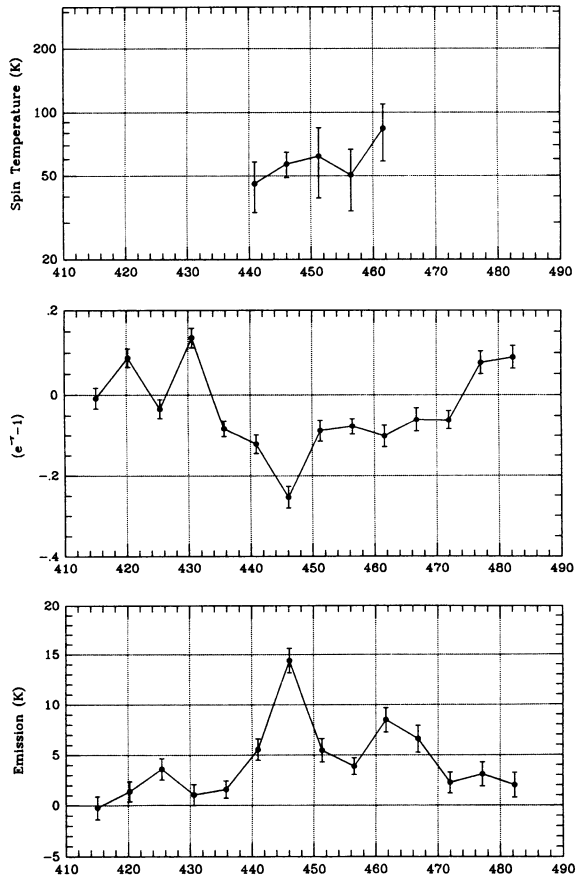

FIG. 10.—Line-of-sight H I absorption (*middle*) and inferred emission (*bottom*) against the continuum source in NGC 4826. Absorption and emission parameters as derived from fitting an elliptical Gaussian of fixed position and dimensions and a background level to each H I channel image at 6″ resolution. Note the implied mean spin temperatures (*top*) of 50–60 K which are similar to the brightest emission detected directly at 9″ resolution (30–40 K). Substantial H I optical depths (of order unity) are likely in the inner disk.

from the major axis (in Figs. 5*a* and 5*c*). Normal galactic disks undergoing circular rotation have a maximum velocity ridge line which is coincident with the major axis and a smooth, linear appearance of position-velocity diagrams made parallel to the major axis. The extraction of kinematic and geometrical parameters of the neutral gas distribution is strongly dependent on which degrees of freedom are allowed in fitting the velocity-field data to a kinematic model. During the last 10 years it has become customary to assume pure rotation of gas within a thin disk and to solve independently for the kinematic parameters in a series of concentric annular zones: the so-called tilted ring model (e.g., Begeman 1989). In practice, a mean kinematic center and systemic velocity are first derived. These are subsequently held fixed while solving for the rotation velocity, inclination, and position angle of the receding line of nodes in a series of concentric annular rings. Experience has shown that many galaxies are kinematically well behaved in the context of this model, displaying relatively constant derived inclinations and position angles over much of the disk and no systematic residuals from the fit. On the other hand, there are circumstances when the degrees of freedom offered by this model are sufficient to represent the data, but the derived quantities vary so widely as a function of radius that their physical relevance becomes questionable. The rather wild variation of the fit parameters seen at radii between 100″ and 300″ in Figure 3 motivates us to reconsider the assumptions inherent in this kinematic model.

If the outer gaseous disk in NGC 4826 is both coplanar and counterrotating with respect to the stellar disk, it is quite conceivable that a kinematic signature of this circumstance may be visible. Any population of stars is expected to have some degree of mass loss. Massive stars will of course experience energetic mass loss from stellar winds during their short lifetime, as well as the expulsion of some significant fraction of their main-sequence mass in a supernova event (of Type Ib or II). But even relatively low mass stars will eventually return a significant fraction of their mass to the interstellar medium via red giant winds, planetary nebulae expulsion and in some cases supernovae of Type Ia. Various estimates of the mass-loss rate from the old stellar populations in S0 and elliptical galaxies are consistent within a factor of 2 (e.g., Faber & Gallagher 1976; Sarazin 1989) with $\dot{M}/L_B = 0.015\ M_\odot\ \mathrm{yr}^{-1}\ (10^9\ L_\odot)^{-1}$. Since the stellar mass loss will carry with it the angular momentum of the stellar rotation, and the occurrence of supernovae should ensure that this gas achieves a reasonably large cross section, a counterrotating gaseous disk should experience deceleration roughly proportional to the local mass-loss rate. The decelerated gas should then experience infall toward the nucleus.

In order to test this hypothesis, we extended the standard tilted ring model outlined above to include a term for radial expansion or contraction in the plane of the galaxy. The kinematic center and systemic velocity derived previously were retained as well as the inclination and the position angle of the receding line-of-nodes that had been found in the unperturbed portion of the outer disk (see Fig. 3), namely 60° and 125°, respectively. The only free parameters used in fitting the velocity field shown in Figure 1 were the tangential and radial velocities as function of radius in the plane of the galaxy. Although this fit was carried out with only these two free parameters instead of the more usual three free parameters for which solutions are shown in Figure 3, the fit residuals were similarly small, with an identical mean value. The results of the fit are

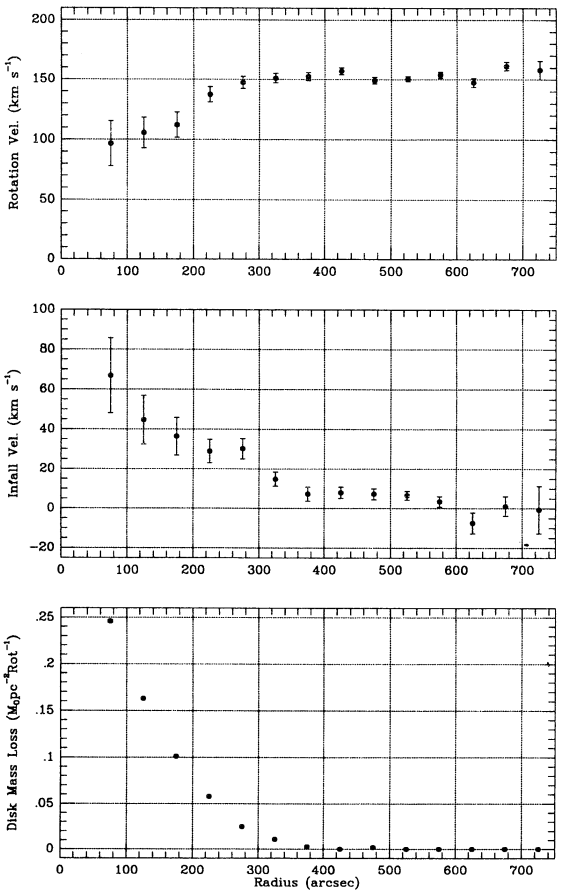

FIG. 11.—Kinematic parameters of the outer disk. Solutions for rotation velocity (*top*) and infall velocity in a tilted ring model of the outer disk at fixed position angle (125°) and inclination (60°). The expected mass loss per unit area per rotation period from an old stellar disk population is given in the *bottom panel* based on the blue light profile and an assumed unperturbed rotation velocity of 150 km s^{-1}. Note the smoothly decreasing rotation velocity and increasing infall velocity between 300″ and 100″ which both appear to track the expected deceleration due to stellar mass loss.

shown in the top two panels of Figure 11. A smoothly decreasing rotation velocity is derived inside of ~300″ radius, accompanied by an increasing infall velocity. By a radius of 100″, the decrement in the rotation velocity and the infall velocity are both ~50 km s^{-1}. This continuous behavior of the values which were fitted independently at each radius is in contrast to the rather nonphysical variation of position angle, inclination, and rotation velocity seen at radii between 100″ and 300″ in the more "conventional" solution of Figure 3.

The blue light profile from our broad-band photometry was normalized with the integrated, extinction-corrected blue magnitude, $B_T^o = 8.96$ mag (de Vaucouleurs, de Vaucouleurs, & Corwin 1976) and a solar $M_B = 5.41$ mag to obtain the mean face-on surface brightness as a function of radius in the outer disk. (This surface brightness varied from ~300–10 $L_\odot$ pc^{-2} between 75″ and 300″.) Scaling with an assumed mass-loss rate of $\dot{M}/L_B = 0.015\ M_\odot\ \mathrm{yr}^{-1}(10^9\ L_\odot)^{-1}$ and the local rotation period assuming an unperturbed rotation velocity of 150 km s^{-1} yields the mass-loss rate profile shown in the lower panel of Figure 11. Significant mass-loss rates of between 0.25 and 0.015 $M_\odot$ pc^{-2} per rotation period are expected between 75″ and 300″. Comparison of these rates with the total gas surface

density in the outer disk, which is quite uniformly 0.5 $M_\odot$ pc^{-2}, suggests that both the magnitude and form of the effect are consistent with the observed perturbation. In particular, at a radius of 150 arcsec we expect a stellar mass-loss rate of $\sim$0.13 $M_\odot$ pc^{-2} per rotational period and measure a gas surface density of 0.65 $M_\odot$ pc^{-2}, so that we would expect a 20% deceleration per rotation period (of 115 Myr) assuming complete coupling of the two gas distributions. The fit shown in Figure 11 indicates a rotation decrement of $\sim$40 km s^{-1}, or $\sim$25% of 150 km s^{-1} at this radius.

It is presumably also relevant that the region of diffuse arcs of Hα emission and high ratio of [S II] to Hα line strength between 60″ and 150″ radius, which was noted above in § 3.2, is coincident with the region of highest expected deceleration of the outer disk and subsequent velocity reversal to that of the inner disk system. These dynamical effects should also be accompanied by soft X-ray emission from the expected shocks as well as the optical emission line ratios characteristic of collisional ionization.

Alternate kinematic models which could be considered in fitting the observed velocity field might include elliptical rather than circular gas orbits such as might be produced by a triaxial potential. While this is in general an interesting and relevant approach, the extremely compact and low-luminosity bulge in NGC 4826 and absence of any extended stellar bar (Walterbos et al. 1994) argue against the physical relevance of such a model in this case.

In summary, it seems very likely that we are indeed observing deceleration of the tenuous, counter-rotating outer gas disk by interaction with the mass lost from the stellar disk. Given the efficiency of this deceleration mechanism, the currently postulated configuration of coextensive counterrotating gas and stars is only likely to survive for another 5–10 rotations or $\sim$1 Gyr. Gas at larger radii than the extent of the stellar disk will not be significantly effected by this mechanism and could consequently survive indefinitely.

4.5. *Origin*

As already noted in BWK92, it is difficult to imagine an intrinsic origin for the counterrotating gaseous disks which we observe within NGC 4826. All of the evidence seems to suggest that this is a relatively short-lived or at least externally induced phenomenon. The observed configuration of nested, counterrotating gaseous disks has been predicted by recent numerical simulations in which two galaxies of antiparallel spin undergo a merger. The most relevant simulation published to date is that of Hernquist & Barnes (1991, hereafter HB91), who consider both the stellar and gas dynamics as well as gas cooling during an encounter of two identical galaxies having the bulge:disk:halo mass ratios of 1:3:16 and a 10% disk mass in gas. The galaxies have antiparallel spins and approach each other in a plane nearly perpendicular to their spin vectors. Approximately 1 Gyr (depending on the original galaxy masses and scale lengths) after the initial encounter at an impact parameter of $\sim$15 kpc the simulated galaxies have settled into a merged (semi-)equilibrium state consisting of two nested counterrotating gaseous disks which are misaligned by $\sim$10°. The inner disk is a factor of 7 smaller than the outer disk but contains $\sim$60% of the gas mass. Scraps of diffuse gas continue to settle into the system from larger radii and scale heights.

Comparison of the line-of-sight velocity distribution shown in Figure 2*b* of HB91 with our Figure 5 reveals the remarkable similarity in predicted and observed gas kinematics. Similarly, a comparison of the face-on distribution of the gas shown in Figure 1*b* of HB91 with our Figure 2 and Figure 4 shows the same dense inner disk, surrounded by a very tenuous outer disk. Our observed ratio of radii is actually $\sim$10 while the mass fraction of gas in the inner disk is 53%. Even the diffuse scraps of gas falling into the simulated disk at large radii seem to have a counterpart in the faint southern tail seen in Figure 1.

The stellar distribution in NGC 4826 is quite different than in the merger remnant of HB91. The semi-equilibrium stellar distribution in the simulation is described as "photometrically similar to an elliptical galaxy." Our broad-band photometry (Walterbos et al. 1994), on the other hand, appears to be dominated by an approximately exponential light profile which is normally interpreted as originating in a stellar disk. Since the stars in the entire disk share the kinematics of the inner gas disk, one possible scenario would appear to be that a gas-poor spiral has undergone an antiparallel spin, approximately coplanar merger with a star-poor dwarf, each containing a few times 10^8 $M_\odot$ of gas. In this way, the stellar disk could be maintained without excessive damage while the gas-gas interaction would remove angular momentum from the gas and allow its infall into the compact inner disk configuration. In this scenario the inner gas disk would consist for perhaps $\frac{2}{3}$ of (high-metallicity) gas from the original spiral and $\frac{1}{3}$ of gas from the dwarf, while the outer gas disk would consist primarily of (low-metallicity) gas from the dwarf. In view of the likely ratio of progenitor masses (of at least visible matter) this scenario might also be referred to as a case of satellite capture.

However, the discussion of the outer disk kinematics above brings at least one other scenario to mind. Rather than postulating a discrete "merger" or "accretion" event in the recent history of NGC 4826 perhaps a more continuous accretion of gas with an opposite sense of angular momentum could explain the complete configuration of components now seen. Comparable gas masses (of a few times 10^8 $M_\odot$) and time scales (of order a Gyr) could conceivably produce a comparable result even if the addition of matter were not "impulsive." The source for such infalling matter could be a primordial halo as envisaged by Quinn & Binney (1992), who even predict a high likelihood for reversals in the sense of angular momentum for external shells of matter. Further numerical simulations and analytic calculations, especially including the dynamical effects of stellar mass loss on gas distributions, would be extremely valuable in assessing this and other possible scenarios.

4.6. *Relevance to Other Systems*

NGC 4826 has demonstrated how the dissipation of angular momentum, presumably as a result of a merger or accretion event of antiparallel spin gas, can lead to efficient fueling of a circumnuclear disk which undergoes vigorous star formation. The obvious question which this begs is: How important has this mechanism been in precipitating nuclear starbursts both in the local universe and during the quasar epoch at redshifts $z = 2$–3 when galaxy interactions were presumably much more frequent and primordial accretion was more substantial? We have begun to address this question by undertaking a survey of the gas kinematics of a large sample of noninteracting nuclear starburst galaxies in order to search for the signature of such events: the presence of counterrotating, gaseous disks. Although a number of optical spectroscopic surveys and a few high-resolution CO studies have delineated the gas kinematics in the inner regions of such systems, the outer disk kinematics have received very little attention to date.

Our possible detection of the effects of stellar mass loss on the outer disk of NGC 4826 raises a number of additional issues. Most directly perhaps is the possibility that NGC 4826 itself will have a rather different appearance in a Gyr's time. The region of overlap of the gaseous disk with the stellar disk should have been swept clean by then, leaving only an external ring of gas counter-rotating with respect to the stellar component, much like that seen in IC 2006 by Schweizer et al. (1989). In other systems, at intermediate times, it should be possible to detect the deceleration and infall of any gaseous component which overlaps a stellar one with different kinematics. This should be very relevant to the class of polar ring galaxies (e.g., Whitmore et al. 1987) and may account for some of the peculiarities observed in their kinematics (e.g., Sackett & Sparke 1990) without the need for invoking significant flattening of a dark halo potential.

Finally, the effects of this mechanism may be visible whenever a gaseous disk is co-extensive with a stellar bulge, since the lower net angular momentum of the bulge should always induce some deceleration in the gas. To estimate the magnitude of this effect consider that the average blue stellar disk surface brightness at small radii is ~ 21.5 mag arcsec^{-2}, while the average extinction is ~ 0.5 mag. A surface brightness of 21 mag arcsec^{-2} corresponds to 250 $L_\odot$ pc^{-2}. A typical rotation velocity for a major galaxy of 200 km s^{-1} at 1.5 kpc radius gives rise to a rotation period of 45 Myr. A stellar mass-loss rate of $\dot{M}/L_B = 0.015\ M_\odot\ \mathrm{yr}^{-1}\ (10^9\ L_\odot)^{-1}$ then results in a local mass injection rate of 0.17 $M_\odot$ pc^{-2} per rotation period. The light of a stellar bulge (if present) and its associated mass loss may be factors of 10 larger at smaller radii, but the mass injection will presumably occur in a thicker distribution than that of a gaseous disk. In any case, when gas surface densities as low as a few $M_\odot$ pc^{-2} are present at radii less than ~ 1 kpc, an observable deceleration should be seen. The physical consequence of this interaction will be the continuous fueling of the nuclear region with gas from the disk. A possible interpretational consequence of this effect might be an artificially low apparent rotation velocity at small radii which might have substantial implications for global models of the galactic mass distribution. A reanalysis of the kinematics of gaseous disks within existing databases might be quite interesting in this regard.

It is a pleasure to acknowledge useful discussion and correspondence with J. van Gorkom, R. Sancisi, T. van der Hulst, L. Hernquist, and H. W. Rix. We thank the NRAO, NOAO, NFRA, and JCMT PATT for their allocations of telescope time, A. Harris for his help in carrying out the JCMT observations and K. Begeman for his help in modifying the velocity-field fitting software. The National Optical Astronomy Observatories is operated by the Association of Universities for Research in Astronomy under cooperative agreement with the National Science Foundation. The James Clerk Maxwell Telescope is operated by the Royal Observatory Edinburgh on behalf of the UK Science and Engineering Research Council (SERC), the Netherlands Organization for Scientific Research (NWO), and the Canadian National Research Council. R. A. M. W. acknowledges grant support from the NSF through grant number AST 91-23777. R. C. K. acknowledges grant support from the NSF through grant number AST 90-19150.

REFERENCES

Begeman, K. G. 1989, A&A, 223, 47
Bender, R. 1990, in Dynamics and Interactions of Galaxies, ed. R. Wielen (Berlin: Springer), 232
Bertola, F., Bettoni, D., Buson, L. M., & Zeilinger, W. W. 1990, in Dynamics and Interactions of Galaxies, ed. R. Wielen (Berlin: Springer), 249
Bloemen, H. 1989, ARA&A, 27, 469
Braun, R. 1988, Millimeter Array Memo., No. 46, NRAO
———. 1990, ApJS, 72, 755
———. 1991, ApJ, 327, 54
Braun, R., & Walterbos, R. A. M. 1992, ApJ, 386, 120
Braun, R., Walterbos, R. A. M., & Kennicutt, R. C. 1992, Nature, 360, 442 (BWK92)
Condon, J. J., Frayer, D. T., & Broderick, J. J. 1991, AJ, 101, 362
Cornwell, T. J. 1988, A&A, 202, 316
de Vaucouleurs, G. 1975, in Galaxies and the Universe, ed. A. Sandage, M. Sandage, & J. Kristian (Univ. of Chicago Press), 557
de Vaucouleurs, G., de Vaucouleurs, A., & Corwin, H. G. 1976, Second Reference Catalogue of Bright Galaxies (Austin: Univ. Texas Press)
Duric, N., Bourneuf, E., & Gregory, P. C. 1988, AJ, 96, 81
Faber, S. M., & Gallagher, J. S. 1976, ApJ, 204, 365
Franx, M., Illingworth, G., & Heckman, T. 1989, ApJ, 344, 613
Hernquist, L. E., & Barnes, J. E. 1991, Nature, 354, 210 (HB91)
Hummel, E., Van der Hulst, J. M., Keel, W. C., & Kennicutt, R. C. 1987, A&AS, 70, 517
Keel, W. C. 1983, ApJ, 268, 632
Kennicutt, R. C. 1983, ApJ, 272, 54
Kennicutt, R. C., & Kent, S. M. 1983, AJ, 1094
Kormendy, J. 1992, in Galactic Bulges, ed. H. Habing & H. Dejonghe (Dordrecht: Kluwer), in press
Quinn, T., & Binney, J. 1992, MNRAS, 255, 729
Rice, W., et al. 1988, ApJS, 68, 91
Rix, H.-W., Franx, M., Fisher, D., & Illingworth, G. 1992, ApJ, 400, L5
Rix, H. W., et al. 1994, in preparation
Rubin, V. C., Graham, J. A., & Kenney, J. D. 1992, ApJ, 394, L9
Rubin, V. C., Burbidge, E. M., Burbidge, G. R., & Prendergast, K. H. 1965, ApJ, 141, 885
Sackett, P. D., & Sparke, L. S. 1990, ApJ, 361, 408
Sage, L. J., & Isbell, D. W. 1991, A&A, 247, 320
Sandage, A., & Tammann, G. 1981, A Revised Shapley-Ames Catalog of Bright Galaxies (Washington, DC: Carnegie Inst. of Washington)
Sarazin, C. L. 1989, in The Interstellar Medium in Galaxies, ed. H. A. Thronson & J. M. Shull (Dordrecht: Kluwer), 201
Schweizer, F. 1982, ApJ, 252, 455
———. 1993, in Physics of Nearby Galaxies: Nature or Nurture? ed. T. X. Thuan, C. Balkowski, & J. Tran Thanh Van, p. 283
Schweizer, F., Van Gorkom, J. H., & Seitzer, P. 1989, ApJ, 338, 770
Soifer, B. T., et al. 1987, ApJ, 320, 238
Tully, R. B., & Fisher, J. R. 1981, ApJS, 47, 139
Van Driel, W., & Buta, R. J. 1991, A&A, 245, 7
Walker, M. F. 1989, PASP, 101, 333
Walterbos, R. A. M., & Braun, R. 1992, A&AS, 92, 625
Walterbos, R. A. M., Braun, R., & Kennicutt, R. C. 1994, AJ, in press
Whitmore, B. C., McElroy, D. B., & Schweizer, F. 1987, ApJ, 314, 439
Young, J. S., & Devereaux, N. A. 1991, ApJ, 373, 414